NANO LETTERS

pubs.acs.org/NanoLett
Letter

Origin of Exciton–Polariton Interactions and Decoupled Dark States Dynamics in 2D Hybrid Perovskite Quantum Wells

Antonio Fieramosca,*,# Rosanna Mastria,# Kevin Dini, Lorenzo Dominici, Laura Polimeno, Marco Pugliese, Carmela Tania Prontera, Luisa De Marco, Vincenzo Maiorano, Francesco Todisco, Dario Ballarini, Milena De Giorgi, Giuseppe Gigli, Timothy C. H. Liew, and Daniele Sanvitto*

Cite This: *Nano Lett.* 2024, 24, 8240–8247

Read Online

ACCESS | Metrics & More | Article Recommendations | Supporting Information

ABSTRACT: The realization of efficient optical devices depends on the ability to harness strong nonlinearities, which are challenging to achieve with standard photonic systems. Exciton–polaritons formed in hybrid organic–inorganic perovskites offer a promising alternative, exhibiting strong interactions at room temperature (RT). Despite recent demonstrations showcasing a robust nonlinear response, further progress is hindered by an incomplete understanding of the microscopic mechanisms governing polariton interactions in perovskite-based strongly coupled systems. Here, we investigate the nonlinear properties of quasi-2D dodecylammonium lead iodide perovskite (n3-C12) crystals embedded in a planar microcavity. Polarization-resolved pump–probe measurements reveal the contribution of indirect exchange interactions assisted by dark states formation. Additionally, we identify a strong dependence of the unique spin-dependent interaction of polaritons on sample detuning. The results are pivotal for the advancement of polaritonics, and the tunability of the robust spin-dependent anisotropic interaction in n3-C12 perovskites makes this material a powerful choice for the realization of polaritonic circuits.

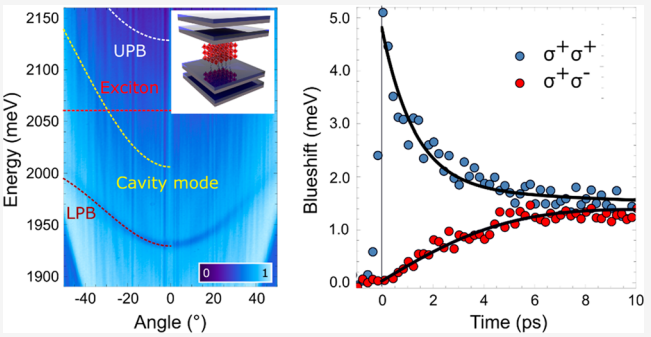

KEYWORDS: *2D perovskite, exciton-polariton, spin-dependent interactions, microcavity polaritons, dark states dynamics*

Over the past two decades, halide perovskites have garnered significant attention and emerged as versatile material platforms for application in various research fields. Their remarkable properties, i.e., direct bandgaps, high optical gain, and strong oscillator strength, combined with high tunability, make them an exceptional platform for customizing specific properties required in different applications.[1−4] In particular, halide perovskites have proven to be excellent candidates for the study of exciton–polaritons, bosonic quasiparticles arising from the hybridization of excitons and photons under strong coupling regime.[5] Owing to their bosonic character, very light effective mass, and strong interparticle interaction, polaritons allow the study of fundamental physics, as well as the realization of all-optical logic devices and low threshold laser sources.[6−8] However, technologically relevant polaritonic devices require RT operation, a criterion that is not fulfilled by III–V and II–VI semiconductors usually employed for polaritonic studies due to their relatively small exciton binding energy. Among high binding energy materials suitable for RT operation,[9] lead-halide perovskites hold a central role. Recent results have shown polariton condensation, parametric scattering, and superfluidity up to RT, with an interaction strength comparable to that of GaAs-based microcavities, that makes perovskites highly attractive.[10−16] In this respect, although many studies have been focused on hybrid organic–inorganic 3D perovskites, 2D perovskites, consisting of inorganic layers of $[PbX_6]^{4-}$ octahedra (with the halogen X = Cl, Br, or I) sandwiched between two layers of organic cations, offer enhanced environmental stability and higher tunability if compared to the 3D counterpart.[17−19] The pronounced quantum confinement experienced by excitons in the natural multiple quantum-well (QW) structure leads to narrow and robust Wannier-Mott-type excitonic transitions. However, such a high binding energy, in general obtained for a single inorganic layer of $[PbX_6]^{4-}$ (n1) surrounded by two organic ones, inevitably leads to a rather small exciton Bohr radius. Increasing the spatial extension of the exciton is crucial for polaritonic applications since the interaction strength depends linearly on the exciton binding energy and quadratically on the

Received: January 29, 2024
Revised: April 8, 2024
Accepted: April 9, 2024
Published: June 26, 2024

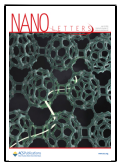

https://doi.org/10.1021/acs.nanolett.4c00418
Nano Lett. 2024, 24, 8240–8247

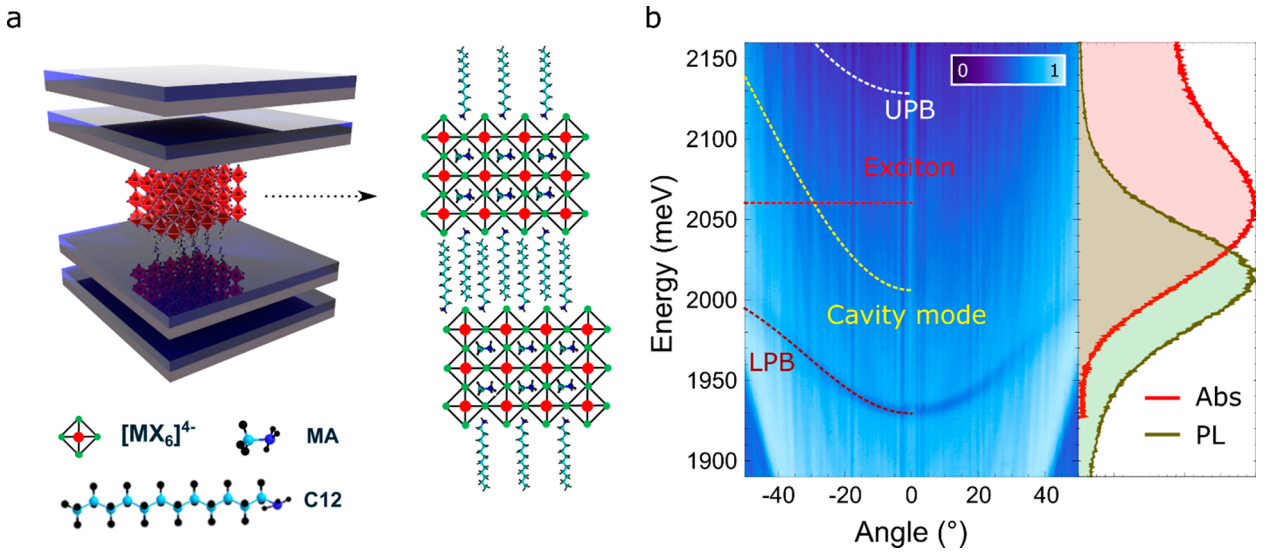

Figure 1. Optical characterization of n3-C12 perovskite microcavity. (a) Schematic of the microcavity, consisting of n3-C12 perovskite single crystals sandwiched between two distributed Bragg reflectors. The structure and chemical composition of the utilized perovskite are provided in the top and bottom parts. (b) Angle-resolved reflectivity map collected on a 400 nm thick crystal. The dashed white and dark-red curves are the UPB and LPB dispersions obtained by using a two-coupled oscillator model to fit the experimental data. The dashed red line and dashed yellow parabola represent the exciton energy and the dispersion of the bare cavity mode, respectively. Absorption (red profile) and photoluminescence (green profile) of the bare crystal are reported in the right inset.

Bohr radius.[20−23] Nevertheless, the quantum confinement can be tailored by varying the number of inorganic layers ($n > 1$), therefore allowing to control these two important parameters.[24] As of today, the integration of high-quality single crystals ($n > 1$) in optical resonators forming stable exciton-polaritons still remains largely unexplored but underpins a central path to further improve the nonlinear response.[5] Moreover, although the presence of strong polariton interactions has been evidenced, a significant gap remains in understanding their microscopic origin. Different mechanisms, including Coulomb exchange interaction, phase space filling (PSF), dipolar interactions, screening of the exciton binding energy, or indirect exchange interaction mediated by biexciton states and/or dark states may contribute to polariton interaction.[25−32] The different microscopic origin behind polariton interaction could be discerned by varying key parameters such as sample detuning, polarization of the pumping laser, and/or employing advanced techniques like pump−probe spectroscopy.[15] Notably, some of these mechanisms are highly spin-dependent and therefore extremely suitable for the realization of polarization-sensitive devices. Understanding the experimental conditions under which spin-dependent nonlinearities play a dominant role is crucial for the development of polariton spintronics, which remains challenging at RT. Here, the nonlinear response of quasi-2D dodecylammonium lead iodide perovskite single crystals, $((C_{12})_2(MA)_2Pb_3I_{10}$ (C_{12} = dodecylammonium, $C_{12}H_{25}NH_3^+$; MA = methylammonium, $CH_3NH_3^+$), with a 3-layer quantum-well thickness (n3-C12) embedded in a planar microcavity has been investigated. Thanks to the extended Bohr radius compared to the 2D counterpart, i.e., phenethylammonium lead iodide perovskite (PEAI) n1, an interaction strength four times higher has been found, therefore demonstrating the ability to tune the interaction by manipulating the chemical composition. More importantly, light is shed on the microscopic origin of polariton nonlinearities, demonstrating that the interactions lose their spin-dependent anisotropy for highly negative exciton−photon detuning. Furthermore, by performing pump−probe measurements, the contribution from long-lived dark-exciton states on polariton interactions is observed and their characteristic spin dephasing time identified.

The sample structure consists of a fully dielectric planar microcavity embedding several isolated single crystals of n3-C12 with different thicknesses, as schematically shown in Figure 1a. The two distributed Bragg reflectors, deposited via e-beam evaporation on a glass substrate, are made of 7.5 pairs of SiO_2/TiO_2 layers each (see SI, Section 1). The n3-C12 crystals, synthesized by using a cooling-induced crystallization approach,[33] are mechanically exfoliated and then transferred on the bottom mirror before the deposition of the top one (see SI, Section 2). Single-crystal X-ray diffraction (XRD) measurements and additional optical characterizations are provided in Figures S1 and S2, respectively.[33,34] Angle-resolved white light reflectance collected on a 400 nm thick crystal, which shows the formation of the lower polariton branch, is reported in Figure 1b. The bare cavity mode dispersion, the upper (UPB) and the lower (LPB) polariton branches, are shown as yellow, white, and dark red dashed line, respectively. The experimental dispersion is well fitted by using a coupled oscillator model in which the exciton energy (red dashed line) is kept at 2060 meV (see right part of Figure 1b), while the energy minimum of the cavity mode is set at E_c = 2006 meV. A Rabi splitting of around 200 meV is retrieved, in good agreement with previous reports.[35,36] The visibility of the UPB is hindered by the strong absorption at high energy, as previously reported.[10,13,37−40] A Transfer Matrix Method (TMM) is employed to simulate the response of the empty microcavity and the coupled one, finding a good agreement, as shown in Figure S3.[41]

In the exciton−polariton framework, nonlinear interactions are strongly spin-dependent, where a stronger (weaker) interaction strength is expected for polaritons with the same (opposite) spin. In inorganic semiconductor QW, polaritons with ±1 spin can be excited because of the electronic band

https://doi.org/10.1021/acs.nanolett.4c00418
Nano Lett. 2024, 24, 8240−8247

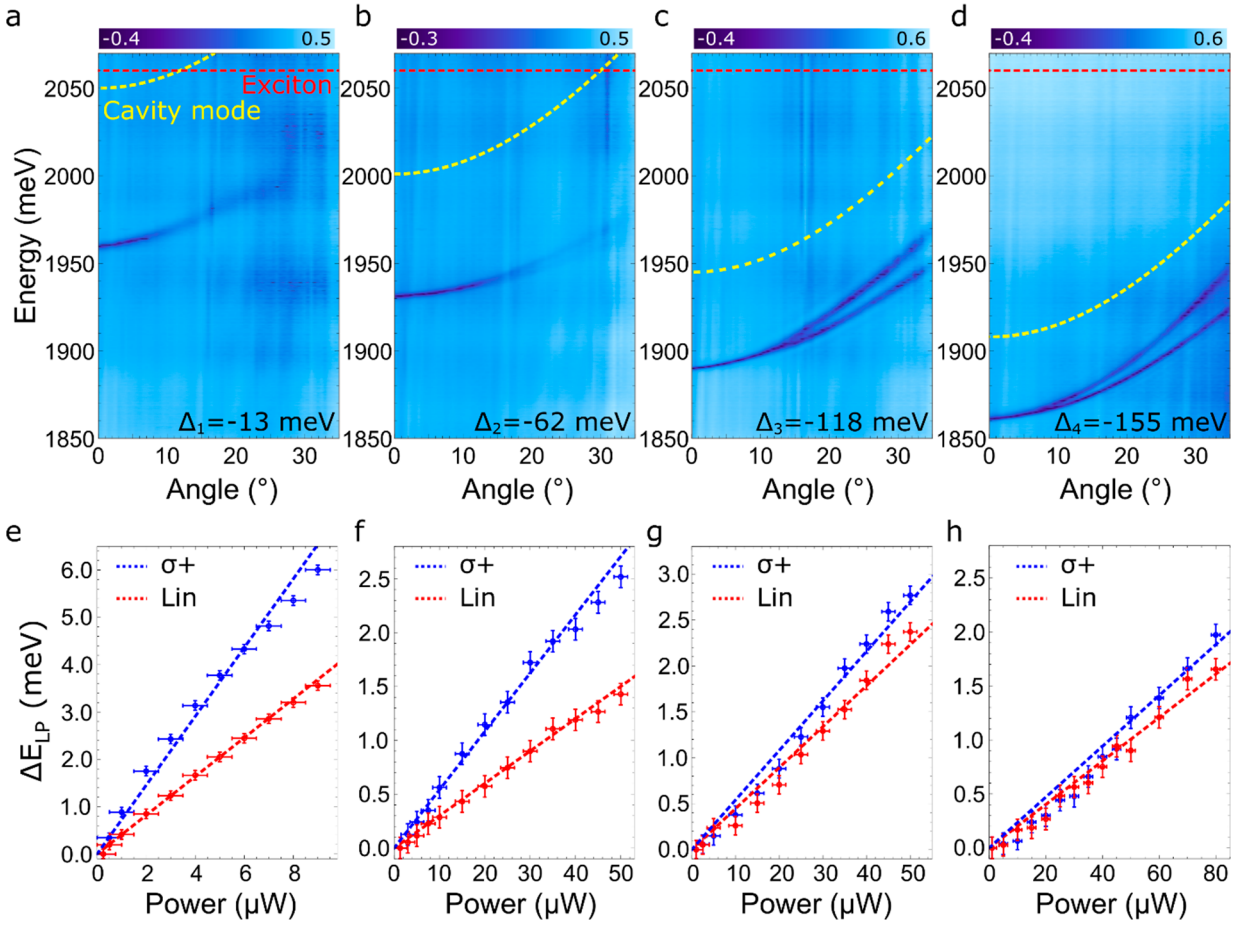

Figure 2. Spin-dependent nonlinearities. (a–d) Angle-resolved reflectivity map collected by using a broadband white light source on samples with different detuning, $\Delta_1 = -13$ meV, $\Delta_2 = -62$ meV, $\Delta_3 = -118$ meV, and $\Delta_4 = -155$ meV, as indicated in the bottom part of (a), (b), (c), and (d), respectively. The dashed yellow parabola and dashed red line indicate the cavity mode and the exciton energy used in the two-coupled oscillator model to fit the experimental LPB dispersion. (e–h) Experimental energy shift of the LPB ground state under resonant excitation as a function of the pumping power for linear (red dots) and circular (blue dots) polarized pumps and for different detuning, as indicated in the top row. The dashed red and blue lines are linear fit of the experimental data. The degree of spin-dependent nonlinearity becomes very small for detuning larger than $\Delta_3 = -118$ meV.

structure in which conservation of angular momentum dictates that spin-polarized excitons can be formed by using either clockwise or counterclockwise circularly polarized light. The same conditions are satisfied for 2D perovskites. Indeed, the electronic structure of both s-type valence band and the p-type conduction band is described by total angular momentum quantum numbers $J = 1/2$ and $J_z = \pm 1/2$, thus the bright excitonic transition satisfies $\Delta J_z = \pm 1$.[42−44] Therefore, polaritons with different spins can be selectively excited by controlling the polarization state of the pumping beam.

Specifically, a linearly polarized pump can be considered as a coherent superposition of two counterpolarized circular components, and consequently, only half of the excited polaritons have the same spin. On the contrary, under circularly polarized laser excitation, all polaritons are created with the same spin, thus leading to a stronger blueshift of the LPB. This spin-dependent anisotropic picture applies if the main source of nonlinearity comes either from Coulomb exchange interaction or PSF[29−31] and it has been theoretically suggested that in 2D perovskite the contribution from PSF is predominant.[45] Although distinguishing between these two types of nonlinearities would require the visibility of the UPB, which is absent in our devices, their spin-dependent anisotropic nature is distinctive, unlike other nonlinearities such as dipolar interactions or screening of the exciton binding energy, which are spin-independent. Therefore, to understand under which experimental conditions spin-dependent nonlinearities play a predominant role, energy-resolved nonlinear transmission measurements are conducted by varying the polarization state of the pumping beam at different detuning values (see SI, Section 3). Specifically, four crystals with different thicknesses have been selected, 380, 400, 415, and 430 nm, resulting in different photon−exciton detuning values, $\Delta_1 = -13$ meV, $\Delta_2 = -62$ meV, $\Delta_3 = -118$ meV, and $\Delta_4 = -155$ meV, as reported in Figure 2a–d, respectively. For all the samples, the dispersion is simulated using a TMM, as reported in Figure S4. The ground state of the LPB is resonantly pumped by using a 100 fs pulse laser, thus avoiding, at low power excitation, the direct formation of an incoherent excitonic reservoir. Notably, the employed perovskite does not exhibit any intrinsic xy optical birefringence, meaning that the LPB dispersion does not show any splitting between two linear components at normal incidence.[46−50] This is particularly important to eliminate any polarization rotation that might affect the polarization state of the pump.

https://doi.org/10.1021/acs.nanolett.4c00418
Nano Lett. 2024, 24, 8240−8247

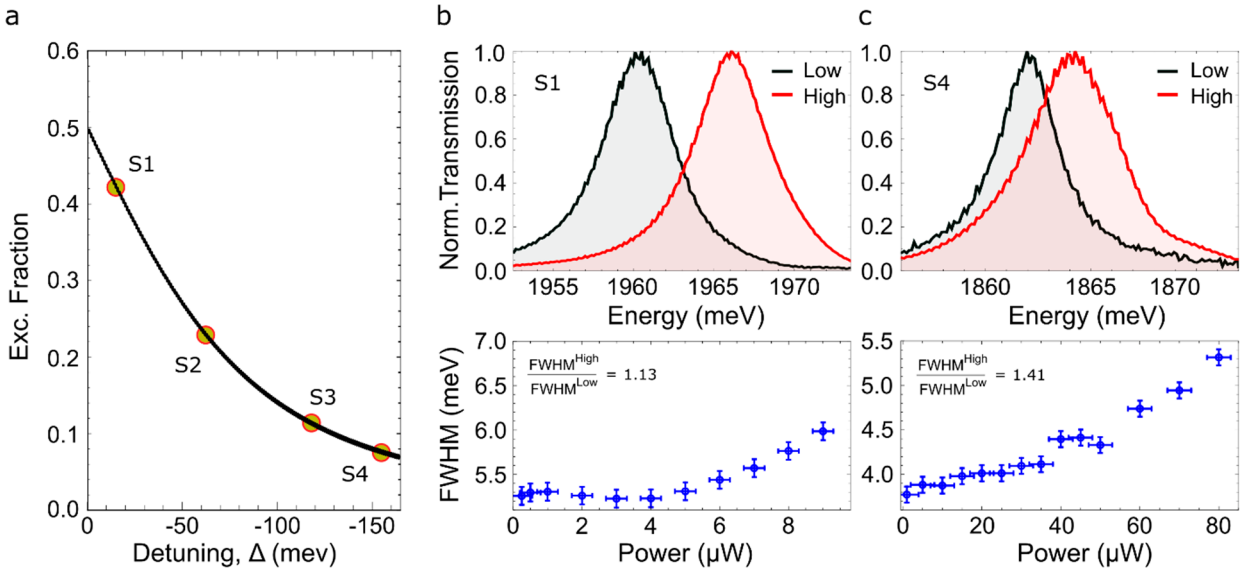

Figure 3. Line width evolution in nonlinear regime. (a) Calculated excitonic fraction of the LPB ground state as a function of the detuning (black solid line). The excitonic fraction of all the samples investigated in this work is shown in Figure 2 by the yellow solid circles, S1, S2, S3, and S4, respectively. (b) Top panel. Normalized energy-intensity profiles of the transmitted pump resonantly injected in the LPB ground state for sample S1 ($\Delta_1 = -13$ meV) and for low (0.2 μW, black profile) and high (9 μW, red profile) pumping power, respectively. Bottom panel. fwhm of the ground state of the LPB as a function of the pumping power. At the highest power used in the experiment a limited broadening of around 13% is visible. (c) Top panel. Same as in (b), but for the most negative detuned sample, S4 ($\Delta_4 = -155$ meV). Low power is 1 μW, while high power is 80 μW. Bottom panel. Same as in (b) bottom panel, but for the most negative detuned sample. At the highest power used in the experiment, a marked broadening of around 41% is visible.

The energy shift of the ground state (ΔE_{LP}) as a function of the pumping power for both linear (red dots) and circular (blue dots, σ^+) polarized pump and different detuning values is reported in Figure 2e–h, respectively. The blueshift for both polarizations is well-fitted by a linear function and, as evidenced by the experimental data, the spin-dependent character disappears for quite negative detuning. Note that the same measurements are also performed by using a σ^- excitation obtaining similar results to that of σ^+ excitation, as shown in Figure S5. Moreover, from the fit of the polaritonic branches, the excitonic fraction of the LPB ground state has been evaluated, which is 0.42 ($\Delta_1 = -13$ meV), 0.23 ($\Delta_2 = -62$ meV), 0.12 ($\Delta_3 = -118$ meV), and 0.08 ($\Delta_4 = -155$ meV), as reported in Figure 3a. Even at high negative detuning, the injected polaritons retain a finite excitonic fraction. Therefore, some spin-dependent nonlinearities are still expected, which instead is not the case for the two most negative detuned samples. To interpret the observed behavior, important insights can be obtained from the analysis of the line width in the nonlinear regime. For small negative detuning ($\Delta_1 = -13$ meV), the blueshift of the LPB is accompanied by a limited line width broadening and the full width at half maximum (fwhm) shows a 13% increase, as reported in Figure 3b. In contrast, for the high negative detuning ($\Delta_4 = -155$ meV), a marked broadening appears and the fwhm shows a 41% increase, as shown in Figure 3c. Therefore, two different regimes can be identified. At small negative detuning (down to $\Delta_2 = -62$ meV), the spin-dependent character and the limited line width broadening immediately suggest that Coulomb interaction and/or PSF are the main source of nonlinearities. In contrast, at high negative detuning, the absence of spin-dependent interactions along with the presence of a marked broadening suggests that second order nonlinear processes are taking place. Specifically, due to the high power needed to observe a suitable blueshift, two photon absorption and Auger recombination become dominant, thus creating an incoherent excitonic reservoir as well as free carriers. Consequently, the polarization is randomized, and the resonant excitation scheme becomes equivalent to an off-resonant excitation performed far from the exciton resonance in the continuum of states. The presence of Auger recombination is demonstrated via time-resolved photoluminescence (TRPL) measurements by pumping the bare perovskite crystals under the same experimental conditions, as reported in Figure S6. A clear nonlinear regime of the TRPL lifetime is visible at high pumping power, comparable to that used for the most negative detuned sample.[51] To corroborate this interpretation, further measurements are performed on the $\Delta_1 = -13$ meV sample upon using off-resonant pumping, to compare these to the clear spin-dependent blueshift (Figure 2e) and limited broadening under resonant excitation (Figure 3b). By using off-resonant pump, although a blueshift of the LPB is observable, the spin-dependent anisotropy disappears, and a marked broadening appears, as shown in Figure S7, thereby confirming our interpretation.

The described picture differs from what has been observed in GaAs sample at cryogenic temperature where, instead, a deviation from the expected spin-dependent anisotropy has been observed at positive detuning, i.e., when the LPB is in resonance with a biexciton state.[25,30] Therefore, our results suggest that, at RT, biexciton mediated interaction can be neglected in quasi-2D n3-C12 perovskite. Moreover, from the data reported in Figure 2e, we have estimated an interaction strength of ≈ 8 μeV μm^2 under circularly polarized excitation, as shown in Figure S8 (see SI, Section 4). This value is roughly four times higher than PEAI n1 thin film[15] and single crystals,[10] thus confirming the higher potential of quasi-2D n3

https://doi.org/10.1021/acs.nanolett.4c00418
Nano Lett. 2024, 24, 8240−8247

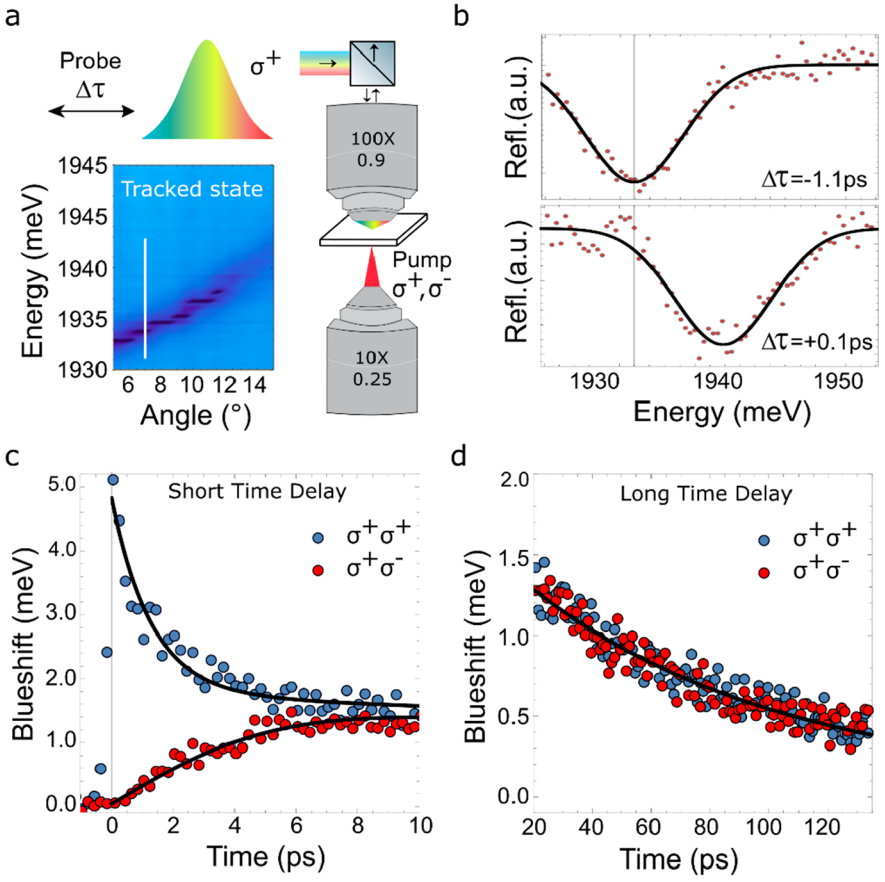

Figure 4. Time resolved pump−probe. (a) Scheme of the experimental configuration. The pump (either σ^+ or σ^-) is kept in the ground state of the LPB in a transmission geometry, while a broadband probe (σ^+) monitors the dispersion at higher energy and higher angles in a reflection geometry. An energy-intensity profile is taken at 7.5 ± 0.3°, as indicated by the white vertical line in the bottom-left inset. (b) An example of the probe spectrum obtained in the co-circular polarized excitation for two pump-probe time delays, $\Delta t = -1.1$ ps and $\Delta t = +0.1$ ps, as reported in the top and bottom part, respectively. The dip in the reflectivity spectrum is fitted with a Gaussian to get the energy position of the LPB. (c) Temporal evolution of the LPB energy shift for the co-circular (blue dots) and cross-circular (red dots) excitation scheme at short time delay (up to 10 ps). The black lines represent the fit of the experimental data following a set of generalized Gross−Pitaevskii equations. (d) Same as in (b), but for long time delay, from 20 to 130 ps.

metal halide-perovskite for the development of RT polariton-based spintronic devices.

To clarify the different states involved in the spin-dependent nonlinearity, we focused our attention on the temporal dynamics of polariton interactions. For a single QW, the eigenstates of the system consist of two bright polariton modes, i.e., the UPB and LPB. When multiple QWs (N_{QW}) are taken into account, the system's eigenstates consist of the same bright polariton modes along with $N_{QW} - 1$ dark states, which are out of phase and decoupled from light.[52−55] Since they are decoupled, these states are long living and lie at the exciton energy, playing a fundamental role in systems with multiple emitters.[28] In this respect, 2D perovskites can be considered a natural multiple QW structure, and as such, the formation of dark $N_{QW} - 1$ states is expected. However, unveiling dark excitations is generally more complex, and their presence can be only indirectly inferred by studying their contribution to polariton interaction by employing, for instance, pump−probe spectroscopy. With this aim, an angle-resolved pump−probe technique is implemented. The pump (either σ^+ or σ^-) is always kept in the ground state of the LPB in a transmission geometry while a weak broadband probe (σ^+) is used to monitor the dispersion at higher energy and higher angles in a reflection geometry. A schematic of the configuration is shown in Figure 4a, while a detailed scheme of the setup is reported in Figure S9. The energy-intensity profile (bottom inset of Figure 4a) has been extracted, and the blueshift of the LPB over time was monitored by fitting the dip in the reflectivity spectrum (see SI, Section 3). An example of the probe spectrum obtained at two different delays, $\Delta t = -1.1$ ps and $\Delta t = +0.1$ ps, is reported in Figure 4b. The LPB blueshift as a function of the time delay for the co-circular excitation scheme (pump σ^+, probe σ^+) is reported in blue dots in Figure 4b and c for short (up to 10 ps) and long time delay (20−130 ps), respectively, for the sample with $\Delta_2 = -62$ meV. A sharp increase in the blueshift is visible within the initial 200 fs, which decreases at long delay times, exhibiting clear biexponential kinetics. The dynamics is characterized by two significantly different decay components, specifically $t_1 = 6$ ps and $t_2 = 60$ ps (see SI, Section 5). Here, the short decay component represents the decay time of the bright polaritons, while the long component represents the decay time of the dark states. Dark states are populated through the scattering of bright polaritons, resonantly injected into the ground state of the LPB. Subsequently, the dark population backscatters into the bright polariton states with a characteristic long decay time, approximately 1 order of magnitude longer than that of the bright ones. This backscattering process results in the

https://doi.org/10.1021/acs.nanolett.4c00418
Nano Lett. 2024, 24, 8240−8247

noticeable blueshift that persists at time delays longer than the bright polariton lifetime. However, different results are obtained with the cross-circular excitation scheme (pump σ^-, probe σ^+), as shown by the red dots in Figure 4b and c. In this excitation scheme, there is no sharp increase in the blueshift. Instead, the blueshift exhibits a gradual rise over time, and after 8 ps, there are no discernible differences between the co- and cross-excitation schemes. This is particularly important because it reveals that the scattering process from bright to dark states randomizes the polarization. Therefore, the indirect exchange interaction assisted by dark states is spin-independent and occurs within the lifetime of the bright polariton states. A scheme showing an energy diagram of the involved processes is reported in Figure S10. The experiments are described considering a standard set of generalized Gross-Pitaevskii equations for the polariton mean-field coupled to an exciton reservoir.[56] The model is fully described in SI, Section 5. The theoretical calculations are overlaid with the experimental points reported in Figure 4c,d, demonstrating excellent agreement. Notably, recent works have proven the importance of $N_{QW} - 1$ dark states in multiple QW polaritonic systems.[52,57] Therefore, although other kinds of dark states, such as high-k dark exciton states, still exist, it is reasonable to assume that in multiple QW systems, the formation of $N_{QW} - 1$ dark states plays a crucial role in the temporal blueshift dynamics. Moreover, we used a bare n3-C12 crystal deposited on a glass substrate and pumped it under the same experimental conditions, as reported in Figure S11. A bleaching of the exciton resonance is visible only when the excitation power is 20 times higher than that used for the microcavity samples, which unambiguously confirms the role of exciton-polaritons in enhancing the nonlinear response. Additionally, the same measurements are conducted on the sample with $\Delta_4 = -155$ meV, as shown in Figure S12. While a second long decay time has been observed, which is compatible with the presence of dark states, no difference is observed between the co- and cross-circular schemes. Specifically, since at high negative detuning the blueshift of the LPB is driven by second order nonlinear processes, the polarization is immediately randomized; therefore, the co- and cross-polarized schemes employed in the pump−probe measurements show the same behavior. The temporal extension of the blueshift observed in our work could potentially overcome the limitations imposed by the short lifetime of state-of-the-art RT microcavities, opening new avenues for manipulating polaritonic states, creating logic devices, and performing neuromorphic computing.[55,58−60]

In conclusion, the microscopic origin of polariton interactions in quasi-2D n3-C12 perovskite single crystals embedded in planar microcavities has been investigated. By performing time-resolved pump−probe measurements, the contribution of the indirect exchange interaction assisted by dark states is observed and a characteristic spin relaxation time is determined. The experimental data are well reproduced by means of a dissipative Gross-Pitaevskii equation for the polariton mean-field coupled to an exciton reservoir. Furthermore, it has been found that the peculiar spin anisotropy in the polariton nonlinearity strongly depends on sample detuning. Coulomb interaction and PSF turned out to play a fundamental role in slightly negative detuning, thus leading to a strong spin anisotropy. On the contrary, second order nonlinear processes, i.e., two photon absorption and Auger recombination, drive the nonlinear response at highly negative detuning, leading to the randomization of polarization and resulting in spin-insensitive nonlinearities. Last, as a technology-oriented result, the evaluated excitonic interaction is four times higher than that of PEAI n1, owing to the extended Bohr radius achieved in n3-C12 perovskite.

The enhanced nonlinear properties, as well as the ability to tailor and control the robust spin-dependent anisotropy of n3-C12 perovskites provide the crucial elements to develop RT polariton-based spintronic devices.

■ ASSOCIATED CONTENT

Data Availability Statement

All data needed to evaluate the conclusions in the paper are presented in the paper and/or the Supporting Information. Additional data related to this paper may be requested from the authors.

Supporting Information

The Supporting Information is available free of charge at https://pubs.acs.org/doi/10.1021/acs.nanolett.4c00418.

Additional information about microcavity fabrication, quasi-2D perovskite synthesis, optical measurements, polariton nonlinearities, theoretical description, XRD pattern, additional optical characterization, TMM simulation of empty microcavity sample, TMM simulation in weak and strong coupling regime, blueshift for different polarization states, TRPL of the bare perovskite crystals, off resonance pumping of $\Delta_1 = -13$ meV sample, interaction constant, angle-resolved pump probe setup, scheme of the involved time-dependent nonlinear phenomena, co-circularly polarized transient absorption of bare perovskite crystals, pump−probe measurements on the sample with $\Delta_4 = -155$ meV, TMM simulation in a broad energy region for different perovskite thickness, and example of pOFF/pON analysis employed in the pump−probe measurements (PDF)

■ AUTHOR INFORMATION

Corresponding Authors

Antonio Fieramosca − *CNR NANOTEC Institute of Nanotechnology, Lecce 73100, Italy;* orcid.org/0000-0002-8912-1137; Email: antonio.fieramosca@nanotec.cnr.it

Daniele Sanvitto − *CNR NANOTEC Institute of Nanotechnology, Lecce 73100, Italy;* orcid.org/0000-0002-3831-8829; Email: daniele.sanvitto@nanotec.cnr.it

Authors

Rosanna Mastria − *CNR NANOTEC Institute of Nanotechnology, Lecce 73100, Italy*

Kevin Dini − *Division of Physics and Applied Physics, School of Physical and Mathematical Sciences, Nanyang Technological University, Singapore 637371, Singapore*

Lorenzo Dominici − *CNR NANOTEC Institute of Nanotechnology, Lecce 73100, Italy;* orcid.org/0000-0002-5860-7089

Laura Polimeno − *CNR NANOTEC Institute of Nanotechnology, Lecce 73100, Italy*

Marco Pugliese − *CNR NANOTEC Institute of Nanotechnology, Lecce 73100, Italy*

Carmela Tania Prontera − *CNR NANOTEC Institute of Nanotechnology, Lecce 73100, Italy;* orcid.org/0000-0002-5934-7733

https://doi.org/10.1021/acs.nanolett.4c00418
Nano Lett. 2024, 24, 8240−8247

Luisa De Marco − *CNR NANOTEC Institute of Nanotechnology, Lecce 73100, Italy;* orcid.org/0000-0002-6855-5438
Vincenzo Maiorano − *CNR NANOTEC Institute of Nanotechnology, Lecce 73100, Italy*
Francesco Todisco − *CNR NANOTEC Institute of Nanotechnology, Lecce 73100, Italy;* orcid.org/0000-0002-0188-6048
Dario Ballarini − *CNR NANOTEC Institute of Nanotechnology, Lecce 73100, Italy*
Milena De Giorgi − *CNR NANOTEC Institute of Nanotechnology, Lecce 73100, Italy;* orcid.org/0000-0002-4522-7933
Giuseppe Gigli − *CNR NANOTEC Institute of Nanotechnology, Lecce 73100, Italy; Department of Mathematics and Physics Ennio De Giorgi, University of Salento, Lecce 73100, Italy*
Timothy C. H. Liew − *Division of Physics and Applied Physics, School of Physical and Mathematical Sciences, Nanyang Technological University, Singapore 637371, Singapore;* orcid.org/0000-0003-2568-7294

Complete contact information is available at: https://pubs.acs.org/10.1021/acs.nanolett.4c00418

Author Contributions

[#]These authors contributed equally to this work (A.F. and R.M.).

Author Contributions

A.F. conceived and designed the experiments. R.M. synthesized the perovskite crystals. A.F., L.D., and L.P. carried out the optical spectroscopy measurements. L.D. developed an automatic LabVIEW code for data acquisition. C.T.P., M.P., V.M., R.M., F.T., and L.D.M. fabricated the samples. K.D. and T.C.H.L. performed theoretical calculations. A.F. wrote the manuscript with contributions from all authors. D.S., G.G., D.B., and M.D.G. supervised the project. All authors discussed the results and commented on the manuscript.

Notes

The authors declare no competing financial interest.

■ ACKNOWLEDGMENTS

The authors gratefully thank P. Cazzato, A. Coriolano, and V. Ardizzone for their valuable technical assistance and fruitful discussions about the data. This work is supported by "Quantum Optical Networks based on Exciton-polaritons" (Q-ONE, N. 101115575, HORIZON-EIC-2022-PATHFINDER CHALLENGES EU project), "National Quantum Science and Technology Institute" (NQSTI, N. PE0000023, PNRR MUR project), "Integrated Infrastructure Initiative in Photonic and Quantum Sciences" (I-PHOQS, N. IR0000016, PNRR MUR project), "Hardware implementation of a polariton neural network for neuromorphic computing" (N. B55F21000600006, Bilateral funding scheme CNR and Russian Foundation for Basic Research), "TECNOMED - Tecnopolo di Nanotecnologia e Fotonica per la Medicina di Precisione" (Ministry of University and Scientific Research (MIUR) Decreto Direttoriale n. 3449 del 4/12/2017, CUP B83B17000010001), "PRIN 22 project NanoPix (2022YM3232), under the PNRR program by the MUR and funded by European Union - Next-Generation EU" and "Ministry of Education (Singapore) via the Tier 3 project MOE2018-T3-1-002".

■ REFERENCES

(1) Yang, D. Toward Stable and Efficient Perovskite Light-Emitting Diodes. *Adv. Funct Materials* **2022**, *32* (9), na.
(2) Kim, J. Y.; Lee, J.-W.; Jung, H. S.; Shin, H.; Park, N.-G. High-Efficiency Perovskite Solar Cells. *Chem. Rev.* **2020**, *120* (15), 7867−7918.
(3) Paulus, F.; Tyznik, C.; Jurchescu, O. D.; Vaynzof, Y. Switched-On: Progress, Challenges, and Opportunities in Metal Halide Perovskite Transistors. *Adv. Funct Materials* **2021**, *31* (29), No. 2101029.
(4) Zhou, Y.; Chen, J.; Bakr, O. M.; Mohammed, O. F. Metal Halide Perovskites for X-ray Imaging Scintillators and Detectors. *ACS Energy Lett.* **2021**, *6* (2), 739−768.
(5) Su, R.; et al. Perovskite semiconductors for room-temperature exciton-polaritonics. *Nat. Mater.* **2021**, *20* (10), 1315−1324.
(6) Sanvitto, D.; Kéna-Cohen, S. The road towards polaritonic devices. *Nat. Mater.* **2016**, *15* (10), 1061−1073.
(7) Deng, H.; Haug, H.; Yamamoto, Y. Exciton-polariton Bose−Einstein condensation. *Rev. Mod. Phys.* **2010**, *82* (2), 1489−1537.
(8) Sanvitto, D. Persistent currents and quantized vortices in a polariton superfluid. *Nature Phys.* **2010**, *6* (7), 527.
(9) Ghosh, S.; et al. Microcavity exciton polaritons at room temperature. *Photonics Insights* **2022**, *1* (1), R04.
(10) Fieramosca, A.; et al. Two-dimensional hybrid perovskites sustaining strong polariton interactions at room temperature. *Sci. Adv.* **2019**, *5* (5), No. eaav9967.
(11) Peng, K.; et al. Room-temperature polariton quantum fluids in halide perovskites. *Nat. Commun.* **2022**, *13* (1), 7388.
(12) Feng, J.; et al. All-optical switching based on interacting exciton polaritons in self-assembled perovskite microwires. *Sci. Adv.* **2021**, *7* (46), No. eabj6627.
(13) Su, R.; et al. Room-Temperature Polariton Lasing in All-Inorganic Perovskite Nanoplatelets. *Nano Lett.* **2017**, *17* (6), 3982−3988.
(14) Polimeno, L.; et al. Observation of Two Thresholds Leading to Polariton Condensation in 2D Hybrid Perovskites. *Adv. Optical Mater.* **2020**, *8* (16), No. 2000176.
(15) Liu, T.; Wang, H.; Song, M.; Zhao, L.; Hu, Z.; Wang, H. Dynamics of Spin-Dependent Polariton−Polariton Interactions in Two-Dimensional Layered Halide Organic Perovskite Microcavities. *Laser & Photonics Reviews* **2022**, *16* (10), No. 2200176.
(16) Wu, J. Perovskite polariton parametric oscillator. *Adv. Photonics* **2021**, *3* (05), na DOI: 10.1117/1.AP.3.5.055003.
(17) Leung, T. L.; Ahmad, I.; Syed, A. A.; Ng, A. M. C.; Popović, J.; Djurišić, A. B. Stability of 2D and quasi-2D perovskite materials and devices. *Commun. Mater.* **2022**, *3* (1), 63.
(18) Coriolano, A.; et al. Improved Photostability in Fluorinated 2D Perovskite Single Crystals. *Nanomaterials* **2021**, *11* (2), 465.
(19) Li, X.; Hoffman, J. M.; Kanatzidis, M. G. The 2D Halide Perovskite Rulebook: How the Spacer Influences Everything from the Structure to Optoelectronic Device Efficiency. *Chem. Rev.* **2021**, *121* (4), 2230−2291.
(20) Ciuti, C.; Savona, V.; Piermarocchi, C.; Quattropani, A.; Schwendimann, P. Role of the exchange of carriers in elastic exciton-exciton scattering in quantum wells. *Phys. Rev. B* **1998**, *58* (12), 7926−7933.
(21) Ciuti, C.; Schwendimann, P.; Quattropani, A. Theory of polariton parametric interactions in semiconductor microcavities. *Semicond. Sci. Technol.* **2003**, *18* (10), S279−S293.
(22) Tassone, F.; Yamamoto, Y. Exciton-exciton scattering dynamics in a semiconductor microcavity and stimulated scattering into polaritons. *Phys. Rev. B* **1999**, *59* (16), 10830−10842.
(23) Glazov, M. M.; Ouerdane, H.; Pilozzi, L.; Malpuech, G.; Kavokin, A. V.; D'Andrea, A. Polariton-polariton scattering in microcavities: A microscopic theory. *Phys. Rev. B* **2009**, *80* (15), No. 155306.
(24) Blancon, J.-C.; et al. Scaling law for excitons in 2D perovskite quantum wells. *Nat. Commun.* **2018**, *9* (1), 2254.

(25) Takemura, N.; Trebaol, S.; Wouters, M.; Portella-Oberli, M. T.; Deveaud, B. Polaritonic Feshbach resonance. *Nature Phys.* **2014**, *10* (7), 500−504.
(26) Togan, E.; Lim, H.-T.; Faelt, S.; Wegscheider, W.; Imamoglu, A. Enhanced Interactions between Dipolar Polaritons. *Phys. Rev. Lett.* **2018**, *121* (22), No. 227402.
(27) Fernandez, H. A.; Withers, F.; Russo, S.; Barnes, W. L. Electrically Tuneable Exciton-Polaritons through Free Electron Doping in Monolayer WS_2 Microcavities. *Advanced Optical Materials* **2019**, *7* (18), No. 1900484.
(28) Ribeiro, R. F.; Martínez-Martínez, L. A.; Du, M.; Campos-Gonzalez-Angulo, J.; Yuen-Zhou, J. Polariton chemistry: controlling molecular dynamics with optical cavities. *Chem. Sci.* **2018**, *9* (30), 6325−6339.
(29) Ballarini, D.; Amo, A.; Viña, L.; Sanvitto, D.; Skolnick, M. S.; Roberts, J. S. Transition from the strong- to the weak-coupling regime in semiconductor microcavities: Polarization dependence. *Appl. Phys. Lett.* **2007**, *90* (20), No. 201905.
(30) Vladimirova, M.; et al. Polarization controlled nonlinear transmission of light through semiconductor microcavities. *Phys. Rev. B* **2009**, *79* (11), No. 115325.
(31) Vladimirova, M.; et al. Polariton-polariton interaction constants in microcavities. *Phys. Rev. B* **2010**, *82* (7), No. 075301.
(32) Suárez-Forero, D. G.; et al. Enhancement of Parametric Effects in Polariton Waveguides Induced by Dipolar Interactions. *Phys. Rev. Lett.* **2021**, *126* (13), No. 137401.
(33) Cinquino, M.; et al. Managing Growth and Dimensionality of Quasi 2D Perovskite Single-Crystalline Flakes for Tunable Excitons Orientation. *Adv. Mater.* **2021**, *33* (48), No. 2102326.
(34) Stoumpos, C. C.; et al. Ruddlesden−Popper Hybrid Lead Iodide Perovskite 2D Homologous Semiconductors. *Chem. Mater.* **2016**, *28* (8), 2852−2867.
(35) Anantharaman, S. B.; et al. Self-Hybridized Polaritonic Emission from Layered Perovskites. *Nano Lett.* **2021**, *21* (14), 6245−6252.
(36) Ouyang, C.; et al. Room temperature exciton-polaritons in high-quality 2D Ruddlesden−Popper perovskites $(BA)_2(MA)_{n-1}Pb_nI_{3n+1}$ (n = 3, 4). *Appl. Phys. Lett.* **2020**, *117* (22), No. 221107.
(37) Łempicka, K.; et al. Exciton-Polaritons in a Tunable Microcavity with 2D-Perovskite. *International Photonics and OptoElectronics Meeting 2019 (OFDA, OEDI, ISST, PE, LST, TSA)*, OSA, Wuhan, 2019; p JW4A.66. DOI: 10.1364/ISST.2019.JW4A.66.
(38) Wang, J.; Su, R.; Xing, J.; Bao, D.; Diederichs, C.; Liu, S.; Liew, T. C.H.; Chen, Z.; Xiong, Q. Room Temperature Coherently Coupled Exciton−Polaritons in Two-Dimensional Organic−Inorganic Perovskite. *ACS Nano* **2018**, *12* (8), 8382−8389.
(39) Fieramosca, A.; et al. Tunable Out-of-Plane Excitons in 2D Single-Crystal Perovskites. *ACS Photonics* **2018**, *5* (10), 4179−4185.
(40) Cinquino, M.; et al. One-step synthesis at room temperature of low dimensional perovskite single crystals with high optical quality. *J. Lumin.* **2020**, *221*, No. 117079.
(41) Song, B.; et al. Determination of Dielectric Functions and Exciton Oscillator Strength of Two-Dimensional Hybrid Perovskites. *ACS Materials Lett.* **2021**, *3* (1), 148−159.
(42) Giovanni, D.; et al. Tunable room-temperature spin-selective optical Stark effect in solution-processed layered halide perovskites. *Sci. Adv.* **2016**, *2* (6), No. e1600477.
(43) Tanaka, K.; et al. Electronic and Excitonic Structures of Inorganic−Organic Perovskite-Type Quantum-Well Crystal $(C_4H_9NH_3)_2PbBr_4$. *Jpn. J. Appl. Phys.* **2005**, *44* (8R), 5923.
(44) Giovanni, D.; et al. Highly Spin-Polarized Carrier Dynamics and Ultralarge Photoinduced Magnetization in $CH_3NH_3PbI_3$ Perovskite Thin Films. *Nano Lett.* **2015**, *15* (3), 1553−1558.
(45) Belogur, A. D.; Baghdasaryan, D. A.; Iorsh, I. V.; Shelykh, I. A.; Shahnazaryan, V. Theory of Nonlinear Excitonic Response of Hybrid Organic Perovskites in the Regime of Strong Light-Matter Coupling. *Phys. Rev. Applied* **2022**, *17* (4), No. 044048.
(46) Polimeno, L.; et al. Tuning of the Berry curvature in 2D perovskite polaritons. *Nat. Nanotechnol.* **2021**, *16* (12), 1349−1354.
(47) Polimeno, L.; et al. Experimental investigation of a non-Abelian gauge field in 2D perovskite photonic platform. *Optica* **2021**, *8* (11), 1442.
(48) Spencer, M. S.; et al. Spin-orbit−coupled exciton-polariton condensates in lead halide perovskites. *Sci. Adv.* **2021**, *7* (49), No. eabj7667.
(49) Łempicka-Mirek, K.; et al. Electrically tunable Berry curvature and strong light-matter coupling in liquid crystal microcavities with 2D perovskite. *Sci. Adv.* **2022**, *8* (40), No. eabq7533.
(50) Chu, Z.; Chen, H.; Mao, X.; Li, Y.; Xu, W.; Ran, G. Anisotropic exciton−polaritons in 2D single-crystalline PEA_2PbBr_4 perovskites at room temperature. *J. Phys. D: Appl. Phys.* **2023**, *56* (10), No. 105301.
(51) Jiang, Y.; et al. Reducing the impact of Auger recombination in quasi-2D perovskite light-emitting diodes. *Nat. Commun.* **2021**, *12* (1), 336.
(52) Zhao, J.; et al. Exciton polariton interactions in Van der Waals superlattices at room temperature. *Nat. Commun.* **2023**, *14* (1), 1512.
(53) Bleu, O.; Li, G.; Levinsen, J.; Parish, M. M. Polariton interactions in microcavities with atomically thin semiconductor layers. *Phys. Rev. Research* **2020**, *2* (4), No. 043185.
(54) Kavokin, A.; Malpuech, G. *Cavity Polaritons*, 1st ed.; Elsevier: San Diego, 2003.
(55) Schmidt, D.; et al. Tracking Dark Excitons with Exciton Polaritons in Semiconductor Microcavities. *Phys. Rev. Lett.* **2019**, *122* (4), No. 047403.
(56) Wouters, M.; Carusotto, I. Excitations in a Nonequilibrium Bose−Einstein Condensate of Exciton Polaritons. *Phys. Rev. Lett.* **2007**, *99* (14), No. 140402.
(57) Chang, W. J.; Zeng, H.; Weatherly, C. T.; Provazza, J.; Liu, P.; Weiss, E.; Stern, N.; Tempelaar, R. Dark State Concentration Dependent Emission and Dynamics of CdSe Nanoplatelet Exciton-Polaritons. *ChemRxiv* **2024**, na.
(58) Tosi, G.; et al. Sculpting oscillators with light within a nonlinear quantum fluid. *Nature Phys.* **2012**, *8* (3), 190−194.
(59) Berloff, N. G.; et al. Realizing the classical XY Hamiltonian in polariton simulators. *Nat. Mater.* **2017**, *16* (11), 1120−1126.
(60) Mirek, R.; et al. Neuromorphic Binarized Polariton Networks. *Nano Lett.* **2021**, *21* (9), 3715−3720.

https://doi.org/10.1021/acs.nanolett.4c00418
Nano Lett. 2024, 24, 8240−8247